

# Conceptual Approaches for Scaling from Molecular to Macroscopic Levels of Nucleation and Precipitation

N. Sahai

*Department of Geology and Geophysics, University of Wisconsin, Madison, 53706, sahai@geology.wisc.edu.*

## 1 INTRODUCTION

### 1.1 *Motivation*

Precipitation and dissolution, by destroying and creating void space, can profoundly alter the fabric of rock, waste-containment canisters, or reactive barriers, thus, impacting mass transfer and fluid flow dynamics in the porous medium. The aims of this study are to determine the molecular-level controls on mineral precipitation, and to examine conceptual approaches for scaling up to the macroscopic level.

### 1.2 *The Problem*

Precipitation may be viewed as two sub-processes, nucleation and crystal growth. Both are path-dependent, and affect precipitation rate. Nucleation, in particular, is poorly understood. At low temperatures, aqueous nucleation can be extremely slow, placing practical limitations on the observation time-scale. Heterogeneous nucleation reduces the time-scale, but added complexities arise such as identification of the type and number of active surface sites. A third problem relates to spatial scales. The earliest formed solid phases are nanometer-sized. Their characterization becomes problematic, because most spectroscopic methods yield atomic level information (Å scale), while traditional microscopic methods work, of course, in the micron size-range. Furthermore, reaction mechanisms are chemically complex. The earliest precipitated phases are often not thermodynamically the most stable (Ostwald Rule of Stages). Worse, thermodynamic stability, itself, is a function of particle size. Precursor phases transform to the most stable form over time. The sequence of aqueous oligomers and solid precursors determines the reaction pathway and, thus, the rate of nucleation and crystal growth. Minor amounts of other dissolved species can also significantly affect the pathway. Finally, even if the chemical complexity is fully appreciated and understood, it is difficult to incorporate the information into a useful form such as a reactive flow model.

### 1.3 *The Approach*

A two-pronged tack is presented here for further discussion and debate. First, I link results of molecular orbital (MO) calculations of energy and vibrational frequencies, for heterogeneous apatite nucleation, to vibrational spectroscopy results. I then suggest links between molecular modeling approaches and microscopy methods. Finally, I review phenomenological models (PM) to nucleation. Values of PM parameters estimated by molecular modeling and spectroscopy/microscopy, can ultimately be incorporated into reactive flow models.

## 2 HETEROGENEOUS APATITE NUCLEATION ON SILICA SURFACE

### 2.1 *Calcium Phosphate Precipitation*

Computational details are provided elsewhere (Sahai and Tossell, 2000; Sahai, 2003). Stable intermediates involved in nucleation were modeled, in consecutive elementary steps, as  $\text{Ca}(\text{H}_2\text{O})_6^{2+}$  adsorption at different surface sites followed by  $\text{HPO}_4(\text{H}_2\text{O})_4^{2-}$  adsorption. The effects of solvation,  $\text{Mg}^{2+}$  and  $\text{H}^+$  were also considered. Realistic constraints were provided by comparing predicted vibrational spectra to experimental spectra.

The silicon three-ring ( $\text{Si}_3\text{O}_6\text{H}_6$ ) was identified as the active site. The most likely reaction pathway involves partial dehydration of the calcium ion leading to inner-sphere adsorption, followed by attachment of  $\text{HPO}_4^{2-}$ , resulting in the formation of a  $\text{CaHPO}_4$  critical nucleus. In terms of model clusters, at circum-neutral pH, the pathway is represented as:  $\text{Si}_3\text{O}_6\text{H}_5(\text{H}_2\text{O})_3^- \rightarrow \text{Si}_3\text{O}_6\text{H}_5\text{Ca}(\text{H}_2\text{O})_6^+ \rightarrow \text{Si}_3\text{O}_6\text{H}_5\text{CaHPO}_4(\text{H}_2\text{O})^-$  (Fig. 1a-c).

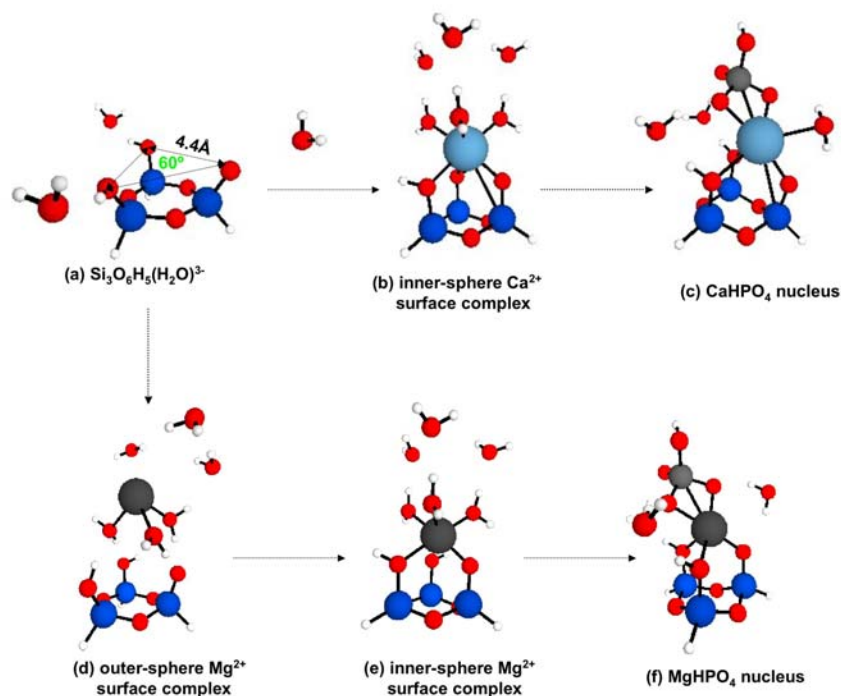


Figure 1. Stable intermediates in amorphous calcium phosphate (a-c) and magnesium phosphate (d-f) nucleation. Heavier arrows for indicate faster elementary steps for one cation than for analogous steps involving the other cation. Legend for atoms: white, H; red, O; dark blue, Si; light grey, P; dark grey, Mg; light blue, Ca.

The electron density associated with surface silanol oxygens, and the geometry of the silanols in the three-ring promote calcium ion dehydration and, thus, formation of the  $\text{CaHPO}_4$  nucleus with bond angles and bond-lengths similar to those in apatite and brushite. Significantly,  $\text{Si}_3\text{O}_6\text{H}_5\text{CaHPO}_4(\text{H}_2\text{O})^-$  and silica reacting with supersaturated solution share unique Infra-Red/Raman bands at 631 and 1125-1145  $\text{cm}^{-1}$ . These peaks are distinct from bands observed in brushite, octacalcium phosphate and crystalline apatite, suggesting that the earliest precursor is amorphous calcium phosphate. Equally important, Si four- and seven-ring surface sites, did not yield  $\text{CaHPO}_4$  clusters with vibrational frequencies similar to experimental spectra.

### 2.3. Kinetic Effects of $\text{Mg}^{2+}$ and $\text{H}^+$

$\text{Mg}^{2+}$  and  $\text{H}^+$ , respectively, are known to inhibit and promote apatite precipitation. The relative rates of  $\text{Mg}^{2+}$  and  $\text{Ca}^{2+}$  adsorption were predicted as  $\text{Mg}^{2+}$  outer-sphere >  $\text{Mg}^{2+}$  inner-sphere >  $\text{Ca}^{2+}$  inner-sphere (Sahai, 2003). It is noteworthy that  $\text{Mg}^{2+}$  sorption is faster than  $\text{Ca}^{2+}$ , despite dehydration for  $\text{Mg}(\text{H}_2\text{O})_6^{2+}$  being slower than for  $\text{Ca}(\text{H}_2\text{O})_6^{2+}$ . The faster adsorption is driven by stronger gas-phase electrostatic attraction of  $\text{Mg}^{2+}$  to the surface site. Hence,  $\text{Mg}^{2+}$  sorbs rapidly, blocking access of nucleating surface sites to  $\text{Ca}^{2+}$ . Furthermore, the outer-sphere  $\text{Mg}^{2+}$  surface complex must convert to the inner-sphere complex before  $\text{HPO}_4^{2-}$  can attach to form the corresponding critical nucleus,  $\text{Si}_3\text{O}_6\text{H}_5\text{MgHPO}_4(\text{H}_2\text{O})_3^-$  (Fig. 1 a, d-f). Comparatively,  $\text{HPO}_4^{2-}$  attachment at the  $\text{Ca}^{2+}$  inner-sphere complex is faster. Apatite nucleation is, thus, retarded but not entirely prevented by  $\text{Mg}^{2+}$ . The geochemical implication

is that the Mg/Ca ratio of solutions does not need to be altered significantly from “normal” compositions by *ad hoc* processes to allow authigenic apatite precipitation. The effects of  $Mg^{2+}$  on crystal growth are beyond the scope of the present paper.

Protons affect nucleation by determining protonation state of the surface site, and of the phosphate ion. The fully protonated and partially deprotonated Si three-ring were capable of nucleating appropriate  $CaHPO_4$  clusters. Moreover, surface charge density ( $\rho$ ) and surface potential ( $\psi$ ) of the nuclei formed depend on solution pH. In turn, interfacial tension ( $\gamma$ ) between two stable nuclei or between nucleus and solution depends on  $\rho$  and  $\psi$  according to the Lippman equation,

$$\frac{d\gamma}{d\psi} = -\rho \quad (1)$$

Interfacial tension should be minimal near the point of zero charge of the mineral, thus promoting crystal growth by expulsion of solution between two nuclei or by “particle bridging” (Schukin and Kontrovich, 1985).

#### 2.4. Estimated Reaction Rates

$Ca^{2+}$  and  $HPO_4^{2-}$  sorption, resulting in nucleation, occurs within minutes to  $\sim 1$  hour. Hydrolysis of the Si 3-ring occurs within  $\sim 24$  hours. Aggregation of oligomers and transformation to apatite crystals large enough to be detected by X-Ray Diffraction is the slowest step, taking about 2 weeks (Sahai and Tossell, 2000).

In summary, a combination of molecular orbital (MO) calculations with experimental spectroscopy can be used to estimate nucleation reaction mechanisms, rate determining steps, and reaction rates.

### 3 PHENOMENOLOGICAL MODELS (PM) OF NUCLEATION

The following discussion on nucleation borrows directly from Stumm (1992), Lasaga (1998), and Steefel and Van Cappellen (1990). Phenomenological models for crystal growth are not considered here for lack of space.

Nucleation of a mineral  $A_\alpha B_\beta$  depends on the degree of supersaturation,  $\Omega$ , which is related to the ion activity product ( $IAP$ ) and macroscopic solubility ( $K_{so}$ ) through:

$$\Omega = \left( \frac{IAP}{K_{so}} \right)^{1/\eta} \quad (2)$$

where,  $\eta = \alpha + \beta$ . For example,  $\eta$  for apatite written as  $Ca_5(PO_4)_3(OH)$  will be different from  $\eta$  for  $Ca_{10}(PO_4)_6(OH)_2$ .

The Gibb’s free energy for nucleation of a cluster containing  $j$  monomers may be represented as the sum of bulk or volume free energy, and surface free energy contributions,

$$\Delta G_j = \Delta G_{bulk} + \Delta G_{surf} = j\Delta G_r + \Delta G_{surf} \quad (3)$$

where  $\Delta G_r$  is the “normal” free energy change for a macroscopic experiment.

*For homogeneous nucleation,*

$$\Delta G_j = -mkT \ln \left( \frac{IAP}{K_{so}} \right) + \gamma_{cw} A_{cw} \quad (4)$$

where  $m = j/\eta$ , is the number of formula units in the nucleating cluster,  $k$  is Boltzmann's constant,  $T$  is absolute temperature,  $\gamma_{cw}$  is the interfacial tension between the critical cluster (stable nucleus) and water, and  $A_{cw}$  is the surface area of the critical cluster in water.

$A$  depends on cluster size and geometry. For example,  $A = 4\pi r^2$ , for a spherical cluster of radius,  $r$ .  $\gamma_{cw}$ , is also size dependent, so macroscopically measured values may not hold at the nanometer size range. Thus, mineral solubility depends on size. The size-dependence becomes significant at small values of  $r$ .

Critical nucleus size, or number of monomers in the critical nucleus is given by,

$$n_c^* \equiv j_c = -\frac{32\pi v^2 \gamma_{cw}^3}{3\Delta G_r^3} \quad (5)$$

where  $v$  is the volume of a monomer. For a spherical nucleus of volume,  $V$ , which is composed of  $j$  monomers,  $v$  is defined as,

$$v = \frac{4}{3\pi} \frac{r^3}{j} = \frac{V}{j} \quad (6)$$

The critical radius is,

$$r_c^* = -\frac{2v\gamma_{cw}}{\Delta G_r} = \frac{2v\gamma_{cw}}{kT\Omega} \quad (7)$$

Activation energy for nucleation is,

$$\Delta G^* = -\frac{16\pi}{3} \frac{\gamma_{cw}^3 v^2}{\Delta G_r^2} = -\frac{16\pi}{3} \frac{\gamma_{cw}^3 v^2}{(kT\ln\Omega)^2} \quad (8)$$

The rate of critical nucleus formation (nucleation rate) is given by

$$J = P \exp\left(\frac{-\Delta G^*}{kT}\right) \quad (9)$$

where the pre-exponential factor,  $P$ , is related to collision efficiency. Thus,  $J$  depends on collision efficiency, extent of supersaturation, interfacial tension, and temperature.

For heterogeneous nucleation, the surface energy contribution to  $\Delta G_j$  is,

$$\Delta G_{surf} = \gamma_{cw} A_{cw} + \left(\gamma_{cs} - \gamma_{sw}\right) A_{cs} \quad (10)$$

where  $\gamma_{cs}$  is the interfacial tension between the critical nucleus and the substrate surface, and  $A_{cs}$  is the surface area of the critical nucleus at the substrate surface. It is, thus, the difference in interfacial tensions between the nucleus at the substrate and the nucleus in solution that drives heterogeneous nucleation. If the geometry of the substrate surface site matches the nucleating crystal, then,  $\gamma_{cs} < \gamma_{cw}$ . For epitaxial templation,  $\gamma_{cs} \rightarrow 0$  and  $\gamma_{sw} \approx \gamma_{cw}$ , so the surface energy term becomes,

$$\Delta G_{surf} = \gamma_{cw} \left( A_{cw} - A_{cs} \right) \quad (11)$$

The critical free energy for heterogeneous nucleation may be approximated as (Steefel and Van Cappellen, 1990),

$$\Delta G^* = -\frac{1\pi}{3} \frac{\gamma_{cw}^3 v^2}{(kT \ln \Omega)^2} \quad (12)$$

The Ostwald-Lussac Rule of Stages is a kinetically driven phenomenon. From Eq. (7) above, we see that at constant  $\Omega$  and  $v$ ,  $r_c^*$  is proportional to  $\gamma$ . Also, it is observed empirically that for ionic solids such as carbonates, oxides and sulfates,  $\gamma_{cw}$  increases as solubility decreases. The most soluble phase, therefore, has the lowest interfacial tension, hence the smallest critical nucleus radius, and the largest nucleation rate. The most soluble phase, therefore, precipitates out first, and eventually transforms to the least soluble (most stable) phase. This explains why the amorphous calcium phosphate precipitates first, and later transforms to apatite.

At supersaturations above the critical value, surface area is generated by nucleation, and at  $\Omega$  values less than critical, new surface area is generated by crystal growth. It is empirically observed that a polydisperse crystal suspension eventually grows to a larger, monodisperse crystal size, a recrystallization process called Ostwald Ripening. The size-dependence of solubility can explain this phenomenon. The smaller crystals are more soluble, hence redissolve, establishing a higher concentration of solutes in their vicinity. Solute concentration is depleted around larger crystals. This establishes a concentration gradient between the two crystals, which drives solute from the smaller towards the larger crystal. Thus, the larger crystal grows at the expense of the smaller ones. Thus, Ostwald Ripening is a thermodynamically driven phenomenon. Other crystal growth mechanisms include attachment of single atoms or oligomers to nuclei, aggregation of stable nuclei by particle bridging, expulsion of solution between adjacent nuclei, and epitaxial templating.

#### 4 ESTIMATING PM PARAMETER VALUES

The discussion above suggests that a description of nucleation requires the knowledge of several model parameters such as interfacial tensions ( $\gamma_{cw}$ ,  $\gamma_{cs}$ ), the size-dependence of these interfacial tension terms, the extent of supersaturation ( $\Omega$ ), and the critical cluster size ( $r_c^*$ ). Similarly, phenomenological models for crystal growth rates, for example, growth by attachment at step-sites, requires knowledge of parameters such as step height, spacing and velocity (e.g., Teng et al., 2000). If these parameters can be estimated or measured, a first approximation to nucleation and crystal growth becomes possible.

For instance, in a solution supersaturated with respect to apatite, the earliest detectable crystals by light scattering experiments, were 0.7-1.0 nm in size (Onuma and Ito, 1998), which we will take as an estimate of the homogenous critical nucleus size. The MO calculations yield  $\sim 0.4$ -  $0.45$  nm for the heterogeneous  $\text{CaHPO}_4$  nucleus (Fig. 1c). We infer that the heterogeneous critical nucleus is a monomer ( $j \sim 1$ ), whereas the homogeneous critical nucleus must be a dimer or trimer of  $\text{CaHPO}_4$ , i.e., that  $j \sim 2$ -3. Further, assuming a spherical nucleus, we estimate  $A_{cs} \sim 2$ - $2.5 \text{ nm}^2$  and  $A_{cw} \sim 6$ - $12 \text{ nm}^2$ . In principle,  $\Delta G_j$  values may be obtained directly from very high-level MO, MD or MC calculations (in practice, accuracy is an issue), and may be combined with the estimated  $A_{cs}$  and  $A_{cw}$ , to obtain values for  $\gamma_{cw}$  and  $\gamma_{cs}$ .

High Resolution Transmission Electron Microscopy and Scanning Probe Microscopy coupled with computational simulation methods such as Molecular Dynamics (MD) or atomistic Monte Carlo (MC) are important for a mechanistic explanation of the nanometer to micron scale observations. Equally significant, microcalorimetric methods, which determine

thermodynamic properties such as heat capacity, entropy, enthalpy and Gibb's free energy of nanoparticles, are important for predicting the relative stability sequence of precursor phases (e.g., Zhang et al., 1999; Majzlan et al., 2000). Finally, a relatively new technique, Vertical Scanning Interferometry, can be coupled with MC simulations to link micron scale processes with the millimeter scale (Lasaga and Lüttge, 2001; Arvidson et al., 2003).

## 5 INCORPORATION OF PRECIPITATION MODELS IN REACTIVE FLOW MODELS

Mass transport by flow through porous media can be simulated using reactive flow models, which account for mass, charge, momentum, and energy balance. The mass balance equations usually contain expressions for total dissolved concentration of solutes ('basis species') distributed among different species such as the uncomplexed basis species, aqueous complexes, surface complexes, ion-exchanged complexes, and precipitated solids (e.g. Yeh and Tripathi, 1991). An additional type of species, "surface precipitates" could be included. A mass action equation with the corresponding equilibrium constant is required to determine the concentration of each species. In order to include nucleation and crystal growth, PM parameters such as  $\gamma_{cw}$ ,  $\gamma_{cs}$ ,  $r_c$ , step height, spacing and velocity, solubility constants ( $K_{so}$ ) as a function of cluster radius, adsorption constants ( $K_{ads}$ ) as a function of adsorbent particle-size, heat capacity, entropy and enthalpy as a function of cluster radius, type and number of reactive surface sites, etc. must be included in the thermodynamic database for the flow model. If cluster size was tracked as the reaction progresses computationally, the relative importance of the size-dependent terms would diminish over time, and it may become possible to "turn off" those terms at some critical value, and allow macroscopic properties to dominate, thus saving on computational time.

In summary, the paper presents the problems associated with modeling precipitation from the molecular level (nucleation) to macroscopic levels (bulk precipitation). Some approaches are presented for tackling these issues.

## REFERENCES

- Arvidson, R.S., Ertan, I.E., Amonette, J.E. and Luttge, A. 2003. Variation in calcite dissolution rates: A fundamental problem? *Geochim. Cosmochim. Acta* **67**, 1623-1634.
- Lasaga, A.C. and Luttge, A. 2001. Variation of crystal dissolution rate based on a dissolution stepwave model. *Science* **291**, 2400-2404.
- Majzlan J., Navrotsky A. and Casey W.H. 2000. Surface enthalpy of boehmite. *Clays. Clay Min.* **48**, 699-707.
- Onuma, K. and Ito, A. 1998. *Chem. Mater.* **10**, 3346-3351.
- Sahai, N. 2003. The effects of  $Mg^{2+}$  and  $H^+$  on apatite nucleation at silica surfaces. *Geochim. Cosmochim. Acta* **67**, 1017-1030.
- Sahai, N. and Tossell, J.A. 2000. Molecular orbital study of apatite ( $Ca_5(PO_4)_3OH$ ) nucleation at silica bioceramic surfaces. *J. Phys. Chem. B.* **104**, 4322-4321.
- Schmidt, M.W. et al. 1993. General atomic and molecular electronic structure system *J. Comput. Chem.* **13**, 1347-1363.
- Schukin, E.D. and Kontorovich, S.I. 1985. Formation of contacts between particles and development of internal stresses during hydration processes. In *Materials Science of Concrete III*, Ed. J. Skalny. The American Ceramic Society, Westerville, OH, 1992, pp. 1-35.
- Steeffel, C.I. and Van Cappellen, P. 1990 A new kinetic approach to modeling water-rock interaction: The role of nucleation, precursors, and Ostwald ripening. *Geochim. Cosmochim. Acta* **54**, 2657-2677.
- Stevens, W.J., Krauss, M., Basch, H. and Jansen, P.G. 1992. Relativistic compact effective core potentials and efficient shared exponent basis sets for the third, fourth and fifth row atoms. *Canad. J. Chem.* **70**, 612-630.
- Stumm, W. 1992. *Chemistry of the Solid-Water Interface*. Wiley, NY, Chapter 6.
- Teng, H.H., Dove, P.M. and De Yoreo J.D. 2000 Kinetics of calcite growth: Surface processes and relationships to macroscopic rate laws. *Geochim. Cosmochim. Acta* **64**, 2255-2266.
- Yeh, G.-T. and Tripathi, V.S. 1991. A model for simulating transport of reactive multispecies components: Model development and demonstration. *Wat. Res. Res.* **27** 3075-3094.
- Zhang H., Penn R.L., Hamers, R.J. and Banfield, J.F. 1999. Enhanced adsorption of molecules on surfaces of nanocrystalline particles. *J. Phys. Chem. B.* **103**, 4656-4662.